

Bond cutting in K-doped tris(8-hydroxyquinoline) aluminium

 Hsin-Han Lee,^a Jennchang Hwang^{a*} and Tun-Wen Pi^b
^aDepartment of Materials Science and Engineering, National Tsing Hua University, Hsinchu 30013, Taiwan, and ^bNational Synchrotron Radiation Research Center, Hsinchu 30076, Taiwan.

E-mail: jch@mx.nthu.edu.tw

A series of Al 2*p*, K 2*p*, O 1*s* and N 1*s* core-level spectra have been used to characterize the interaction between potassium (K) and tris(8-hydroxyquinoline) aluminium (Alq₃) molecules in the K-doped Alq₃ layer. All core-level spectra were tuned to be very surface sensitive in selecting various photon energies provided by the wide-range beamline at the National Synchrotron Radiation Research Center, Taiwan. A critical K concentration ($x = 2.4$) exists in the K-doped Alq₃ layer, below which the K-doped atoms generate a strained environment near the O and N atoms within 8-quinolinoline ligands. This creates new O 1*s* and N 1*s* components on the lower binding-energy side. Above the critical K coverage, the K-doped atoms attach the O atoms in the Al–O–C bonds next to the phenoxide ring and replace Al–O–C bonds by forming K–O–C bonds. An Alq₃ molecule is disassembled into Alq₂ and Kq by bond cutting and bond formation. The Alq₂ molecule can be further dissociated into Alq, or even Al, through subsequent formations of Kq.

Keywords: tris(8-hydroxyquinoline) aluminium (Alq₃); K doping; bond cutting; interface; photoemission.

1. Introduction

In past years, alkali metals and alkali metal compounds have been used as electron injection materials that are doped into electron transport layers in order to improve the performance of organic light-emitting devices (OLEDs) (Parthasarathy *et al.*, 2001; Lee *et al.*, 2005; Ganzorig *et al.*, 2001; Stöbel *et al.*, 2000; Brown *et al.*, 2003). The alkali-metal-doped organic layer is usually formed by depositing an alkali metal layer between the electron transport layer tris(8-hydroxyquinoline) aluminium (Alq₃) and cathode material aluminium (Al). The molecular structure of Alq₃, sketched in Fig. 1, consists of pyridyl and phenoxide rings. The performance of lithium (Li) doped Alq₃ layers near the cathode interface in OLED devices has been intensively studied (Haskal *et al.*, 1997; Kido *et al.*, 1993; Kido & Matsumoto, 1998). Kido & Matsumoto (1998) demonstrated that Li-doped Alq₃ layers are effective in lowering the driving voltage for the electron injection. The Li-doped atoms play a role in donating electrons to the pyridyl ring of Alq₃ such that the conductivity of the Alq₃ layer increases. Recently, another alkali metal, potassium (K), has attracted much attention as it is easier for K to donate electrons compared with Li, owing to the lower ionization energy of K. Fundamental studies on the K-doped Alq₃ layer have been investigated by the valence band and core-level spectra obtained through ultraviolet photoemission spectroscopy and X-ray photoemission spectroscopy (Johansson *et al.*, 1999;

Schwieger *et al.*, 2001). Johansson *et al.* (1999) reported that electron transfer occurred from K to three ligands of the Alq₃, and that a new spectral feature appeared in the valence band. Later, Schwieger *et al.* (2001) reported that a low intercalation of K led to a rigid energy shift for all electronic levels. A high intercalation of K in Alq₃ resulted in structural modification of the Alq₃ molecules by forming an organometallic complex. However, detailed structural modification by the K-doped atoms was not reported. It is of fundamental interest to investigate how the structure modification occurs at the K/Alq₃ interface. A pristine Alq₃ layer is doped with K from low

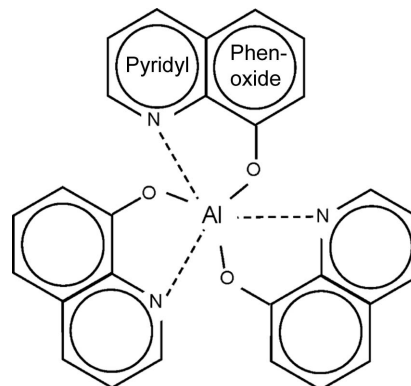


Figure 1
 Schematic drawing of an Alq₃ molecule structure consisting of pyridyl and phenoxide rings.

to high dosage in order to fully understand the interaction between K and Alq₃ at the K/Alq₃ interface.

In this article we present a discovery of bond cutting in the K-doped Alq₃ layer. A series of Al 2*p*, K 2*p*, O 1*s* and N 1*s* core-level spectra were measured *in situ* during the doping of K onto an Alq₃ layer by synchrotron radiation photoemission. With the benefits of strong intensity and surface sensitivity offered by this technique, the cutting of the Al–O–C bonds in the Alq₃ molecule by the K-doped atoms was observed.

2. Experimental

Mirror-polished n-type Si(100) samples ($\rho = 1\text{--}10\ \Omega\ \text{cm}$) were pre-oxidized using the Ishizaka and Shiraki method in order to remove possible carbon contamination (Ishizaka & Shiraki, 1986). The Si(100) samples were then fixed on a rotatable molybdenum sample holder with two pairs of tantalum plates in a photoemission chamber pumping down to a base pressure of $\sim 7 \times 10^{-11}$ torr. In order to remove the protected oxide layer, the Si(100) samples were annealed stepwise up to 1153 K to obtain a clean Si(001) 2×1 surface on which Alq₃ was vacuum-evaporated using an Omicron EFM3 evaporator. The deposition of Alq₃ was recorded by the evaporation time and the evaporation flux of EFM3. The deposition rate of Alq₃ was estimated to be $0.14\ \text{ML}\ \text{min}^{-1}$. K atoms were evaporated from a SEAS getter onto the pre-evaporated Alq₃ layer. The deposition of K was recorded by the evaporation time and the power used to heat the SEAS getter. The K flux out of the SEAS was divergent so it was not possible to estimate the deposition rate of K onto Alq₃. The K concentration in the Alq₃ layer was determined by comparing the relative peak areas of K 2*p* and C 1*s* under various deposition conditions, taking into account their relative cross-section factors. The cross-section factors of K 2*p* and C 1*s* at a photon energy of 330 eV are 2.4 and 0.35, respectively (Yeh & Lindau, 1985). The concentration of K in the Alq₃ layer was expressed as *x* in all the core-level spectra.

The operation pressures during the deposition of Alq₃ and K were maintained below 1.5×10^{-9} and 6×10^{-10} torr, respectively. Normal emission photoelectrons were collected with an Omicron EA125 hemispherical analyzer in the photoemission chamber using the photon energies provided by the wide-range (WR) spherical-grating-monochromator beamline at National Synchrotron Radiation Research Center in Taiwan. Al 2*p*, K 2*p*, O 1*s* and N 1*s* core levels were taken at an incident angle of 70° with their kinetic energies tuned to 40–60 eV, in order to obtain surface-sensitive spectra according to the universal curve (Brundle, 1975). The pass energy of the Omicron EA125 hemispherical analyzer for all the photoelectrons was set to 10 eV. The corresponding electron energy resolution was 0.12 eV. However, the total energy resolution was limited by the photon energy resolution. The

Table 1

Binding energies and Gaussian widths of Al 2*p*_{3/2} components and their corresponding area percentages.

Components	Evaporation time (min)	K concentration (<i>x</i>)	Binding energy (eV) Al 2 <i>p</i> _{3/2}	Gaussian width (eV)	Area percentage (%)
Al- <i>a</i>	0	0	74.49	1.20	100
	3	0.2	74.59	1.39	100
	9	0.7	74.66	1.38	100
	16	1.3	74.78	1.30	100
	21	1.7	74.77	1.37	100
	27	2.1	74.72	1.34	100
	31	2.4	74.64	1.37	90.4
	37	2.9	74.88	1.36	88.8
	45	3.5	74.86	1.35	52.3
	Al- <i>b</i>	31	2.4	73.91	1.36
37		2.9	74.16	1.36	9.3
45		3.5	74.11	1.34	23.5
Al- <i>c</i>	37	2.9	73.36	1.37	1.9
	45	3.5	73.34	1.34	20.5
Al- <i>d</i>	45	3.5	72.61	1.36	3.7

photon energy resolution was affected by the selection of photon energy and the grooves of the spherical grating at the WR beamline. The photon energy resolutions were determined to be 0.16, 0.44, 0.44 and 0.66 eV for photon energies of 136, 330, 440 and 580 eV, respectively. In the analysis of the photoelectron spectra, core-level spectra were normalized

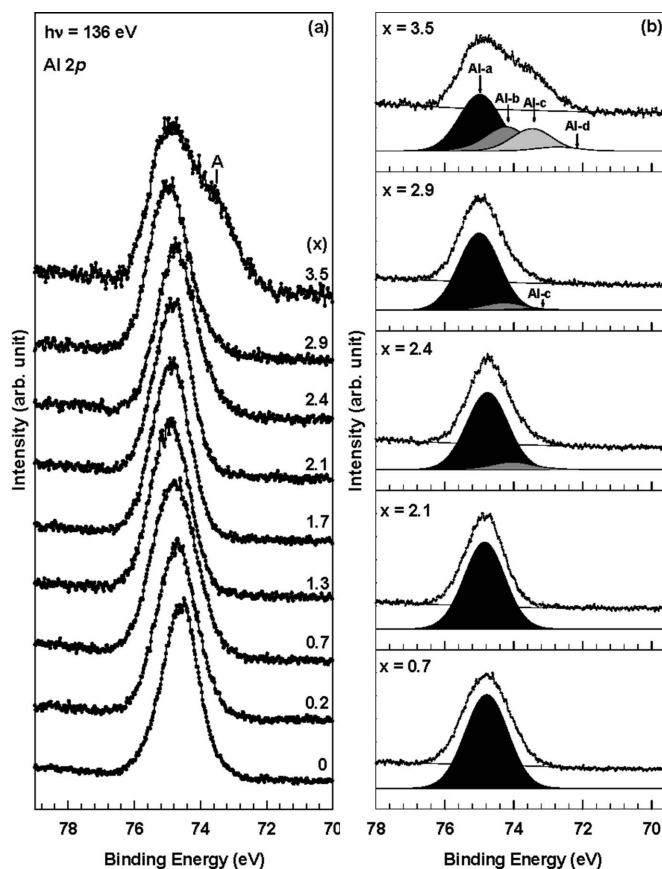


Figure 2

(a) Surface-sensitive Al 2*p* core-level spectra taken *in situ* at a photon energy of 136 eV during deposition of K onto a thick Alq₃ layer. (b) Curve fit of the Al 2*p* spectra in (a).

by the light intensity. The light intensity was characterized by measuring the mesh current at the entrance of the photoemission chamber. No charging problem was observed during the photoemission measurements. A sample of Alq_3 intercalated with Ag was used to determine the Fermi edge since no Fermi edge was observed even at a high intercalation of K into the Alq_3 layer. All the core-level spectra were de-convoluted in a Voigt function and the backgrounds were subtracted in a power-law function by using the curve-fit program *UNIFIT 2006*. The branching ratios of Al $2p$ and K $2p$ were both fixed at 0.5. The spin-orbit splittings of Al $2p$ and K $2p$ were fixed at 0.4 eV and 0.75 eV, respectively. The evolution of the curve-fit in the convolution was plotted separately for all core-level spectra.

3. Results and discussion

Fig. 2(a) shows the surface-sensitive Al $2p$ core-level spectra *in situ* taken at a photon energy of 136 eV during deposition of K onto a thick Alq_3 layer. The Al $2p$ signal from the pristine Alq_3 is located at a binding energy of 74.6 eV with a peak width of 1.2 eV. Upon the deposition of K, the Al $2p$ signal slightly shifts to higher binding energy and its peak width becomes broader (~ 1.4 eV). This is attributed to the band bending resulting from charge donation of K into the lowest unoccupied molecular orbital (LUMO) of the Alq_3 layer (Ishii *et al.*, 1999). Above the critical K concentration (at $x = 2.4$), a new peak (A) begins to appear and becomes an apparent shoulder at a binding energy of ~ 73.6 eV at $x = 3.5$. The shoulder A is about 2 eV in width higher than the Al $2p$ width in pristine Alq_3 (~ 1.2 eV). This indicates that the shoulder A consists of at least two Al $2p$ signals of Al-related oxidation states in organometallic complex at $x = 3.5$. In other words, at least two new Al bonding environments are induced by the doping of K into Alq_3 . The new types of Al bonding environments can be obtained from the deconvoluted data of the Al $2p$ spectra shown in Fig. 2(b), where four Al $2p$ components (Al-a, Al-b, Al-c and Al-d) are required to obtain a consistent fit for all the Al $2p$ spectra. The binding energies and Gaussian widths of the four Al $2p$ components are summarized in Table 1. The curve-fit with three Al $2p$ components is excluded since their Gaussian widths scatter too much. The Al-a peak at a binding energy of 74.6 eV arises from the pristine Alq_3 . The Al-b, Al-c and Al-d peaks are the induced components, which begin to appear at $x = 2.4$, 2.9 and 3.5, respectively. The four Al $2p$ components are strongly correlated to three Al oxidation states (Al^{3+} , Al^{2+} , Al^+) and metallic Al according to their relative energy positions reported in a study of Fe_3Al -type alloys (López *et al.*, 1997). From a chemical perspective the Al-b, Al-c and Al-d components indicate the existence of three different bonding environments for the Al atoms. This supports the bond cutting and bond formation occurring at the Al–O–C bonds next to the phenoxide rings in Alq_3 at $x > 2.4$

Table 2

Binding energies and Gaussian widths of K $2p_{3/2}$ components and their corresponding area percentages.

Components	Evaporation time (min)	K concentration (x)	Binding energy (eV) K $2p_{3/2}$	Gaussian width (eV)	Area percentage (%)
K-a	3	0.2	294.16	1.72	100
	9	0.7	294.31	1.61	100
	16	1.3	294.71	1.63	100
	21	1.7	294.83	1.64	100
	27	2.1	295.07	1.64	100
	31	2.4	294.70	1.62	88.3
	37	2.9	294.90	1.65	78.2
K-b	45	3.5	294.68	1.59	65.6
	31	2.4	295.29	1.73	11.7
	37	2.9	295.50	1.73	21.8
	45	3.5	295.28	1.79	34.4

(critical K concentration) (Burrows *et al.*, 1996). Very probably the Alq_3 molecule is disassembled into Kq and Alq_2 through the formation of Kq at $x = 2.4$. Alq_2 is further dissociated into Alq or even Al through subsequent formations of Kq. Note that the Al $2p_{3/2}$ of the Al-d component is located at a binding energy of 72.6 eV that is consistent with the pure Al metal data (Gredelj *et al.*, 2001). Thus Al-a, Al-b, Al-c and Al-d are assigned as the Al $2p$ signals from Alq_3 , Alq_2 , Alq and Al,

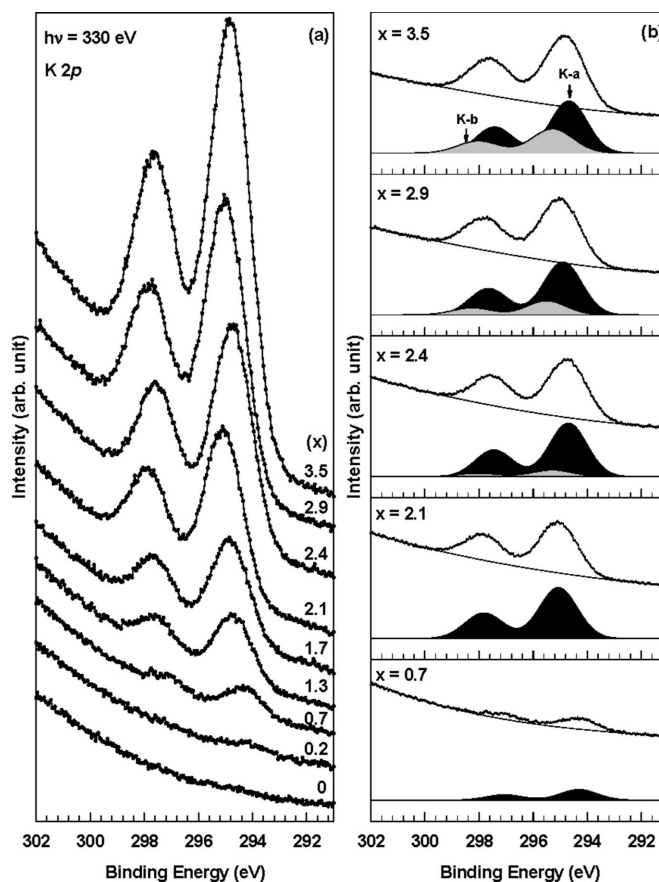


Figure 3

(a) Surface-sensitive K $2p$ core-level spectra taken *in situ* at a photon energy of 330 eV during deposition of K onto a thick Alq_3 layer. (b) Curve fit of the K $2p$ spectra in (a).

respectively. In other words, bond cutting occurs during the doping of K atoms into the Alq_3 layer.

Fig. 3(a) shows the surface-sensitive K 2*p* core-level spectra *in situ* taken at a photon energy of 330 eV during deposition of K onto a thick Alq_3 layer. The K 2*p* signal increases in intensity with deposition time, which agrees well with the amount of K doped into the Alq_3 layer. The energy of K 2*p* also shifts to higher binding energy owing to band bending as observed for the Al 2*p* signals in Fig. 2(a). Similar to the Al 2*p* spectra, the K 2*p* signal becomes broader at $x = 3.5$, indicating the existence of new K bonding environments. The new types of K bonding environments can be obtained by the deconvoluted data of the K 2*p* spectra, where two K 2*p* doublets (K-a and K-b) are required to obtain a consistent fit for all the K 2*p* spectra. The binding-energy values and Gaussian widths of K-a and K-b are listed in Table 2. The bond cutting of Alq_3 by K is also supported by the deconvoluted K 2*p* spectra in Fig. 3(b), where a new K 2*p* doublet (K-b) begins to appear at $x = 2.4$, concurrent with the appearance of the Al-b chemical state in Fig. 2(b). The newly formed doublet K-b is thus assigned as the K 2*p* from Kq since one of the Al-q bonds in Alq_3 is cut *via* the reaction $\text{Alq}_3 + \text{K} = \text{Alq}_2 + \text{Kq}$. The doublet K-a is assigned to the K 2*p* signal from the K atoms doped in Alq_3 before bond cutting (at $x < 2.4$).

Fig. 4(a) shows the surface-sensitive O 1*s* *in situ* core-level spectra taken at a photon energy of 580 eV during deposition of K onto a thick Alq_3 layer. The prominent peak at a binding energy of 531.6 eV is the O 1*s* peak from the pristine Alq_3 . Upon the deposition of K, the O 1*s* signal exhibits an energy shift to higher binding energy, owing to band bending. The line shape of the O 1*s* peak becomes broad and asymmetric at $x > 1.7$. Two new signals B1 and B2 clearly appear at a binding energy of ~ 531 eV ($x = 2.9$) and ~ 529 eV ($x = 3.5$), respectively. The new O 1*s* signals can be further characterized through the deconvoluted data in Fig. 4(b) where three components O-a, O-b and O-c are required to obtain a consistent fit for all the O 1*s* spectra. The binding-energy values and Gaussian widths of the three components are listed in Table 3. The component O-a is assigned from the pristine Alq_3 , which is emitted from the O atoms bonded with Al in Alq_3 . The component O-b starts to appear (Fig. 4b) before bond cutting ($x < 2.4$). This suggests that the O-b component is not from the K-O bonds that form after bond cutting ($x > 2.4$) and will be described later. Very probably the K-doped atoms generate a strained environment near the O atoms in Alq_3 such that the Al-O-C bond angle changes and results in the component O-b. Note that the component O-c starts to appear (Fig. 4b) at $x = 2.4$, the same as the beginning of the bond cutting ($\text{Alq}_3 + \text{K} = \text{Alq}_2 + \text{Kq}$). The component O-c is therefore from the O atom in either Kq or Alq_2 . The component O-c is assigned to the O atom in Kq

Table 3

Binding energies and Gaussian widths of O 1*s* components and their corresponding area percentages.

Components	Evaporation time (min)	K concentration (x)	Binding energy (eV) O 1s	Gaussian width (eV)	Area percentage (%)	
O-a	0	0	531.56	1.54	100	
	3	0.2	531.84	1.75	100	
	9	0.7	532.00	1.70	96.7	
	16	1.3	531.86	1.69	90.9	
	21	1.7	532.03	1.67	79.4	
	27	2.1	532.25	1.64	64.9	
	31	2.4	532.52	1.64	57.0	
	37	2.9	532.29	1.68	31.4	
	45	3.5	532.55	1.62	30.3	
O-b	9	0.7	530.86	1.71	3.3	
	16	1.3	530.70	1.67	9.1	
	21	1.7	530.86	1.66	20.6	
	27	2.1	531.11	1.66	35.1	
	31	2.4	531.38	1.62	38.7	
	37	2.9	531.15	1.71	55.9	
	45	3.5	531.42	1.62	53.3	
	O-c	31	2.4	529.45	1.61	4.3
		37	2.9	529.14	1.65	12.7
45		3.5	529.48	1.60	16.4	

rather than that in Alq_2 , since the O 1*s* in Alq_2 exhibits the same energy as that in Alq_3 based on the following arguments. First, the O 1*s* signal is emitted from the Al-O-C bonds next

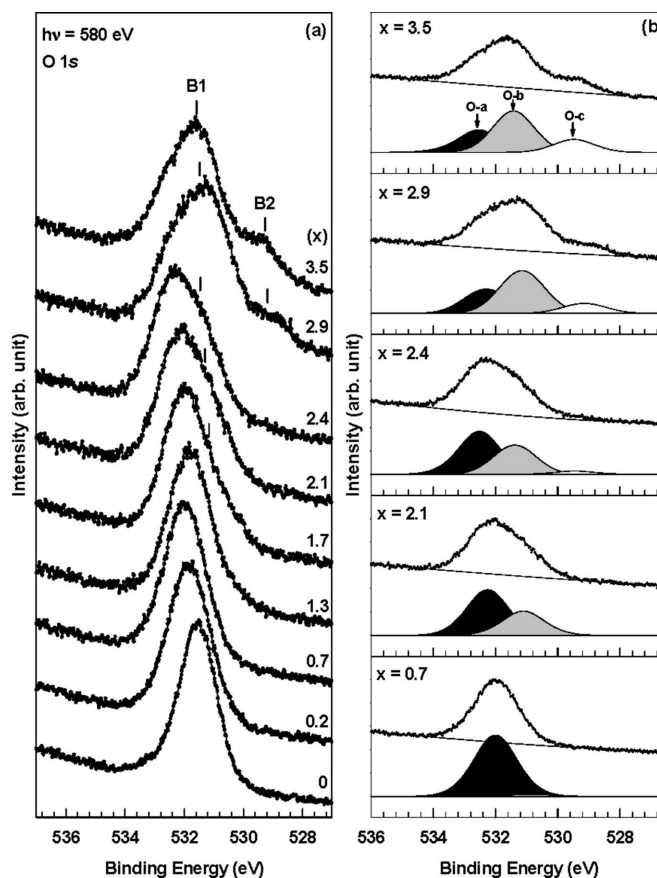


Figure 4
(a) Surface-sensitive O 1*s* core-level spectra taken *in situ* at a photon energy of 580 eV during deposition of K onto a thick Alq_3 layer. (b) Curve fit of the O 1*s* spectra in (a).

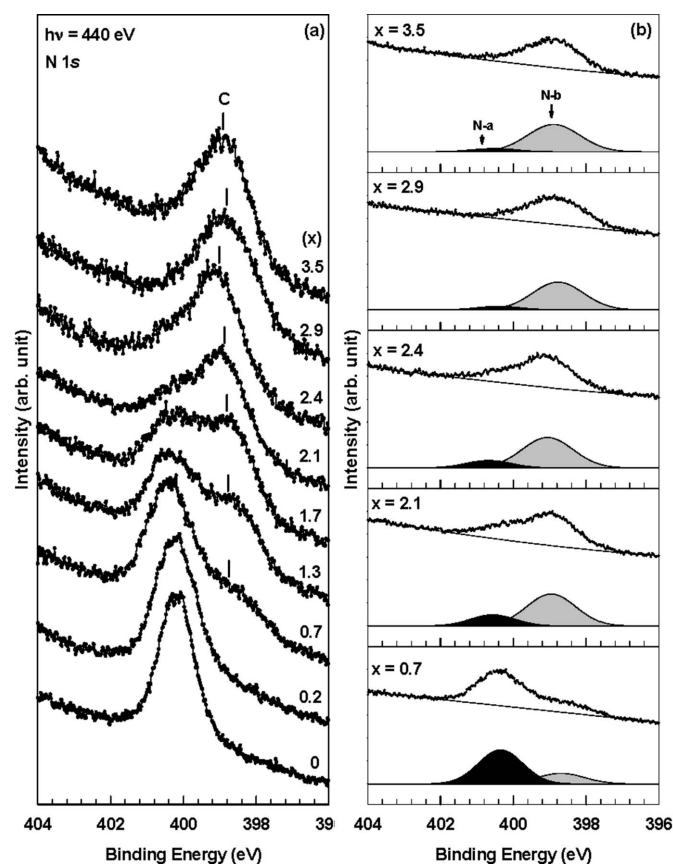
to the phenoxide rings in either Alq₃ or Alq₂. Note that there exist two further reactions, Alq₂ + K = Alq + Kq and Alq + K = Al + Kq, at deposition times longer than $x = 2.4$, according to the Al 2*p* spectra in Fig. 2. If the energy position of O 1*s* in Alq₂ was different from that in Alq₃, three O 1*s* components from Alq₃, Alq₂ and Alq, respectively, should exist. However, no new O 1*s* component appears in subsequent bond cutting occurring at $x = 2.9$ and at $x = 3.5$. This suggests that the induced O 1*s* signals from Alq₂ and Alq may overlap with that from Alq₃ (the O-*b* component). According to the fitted data in Table 3, the amount of O-*b* increases at $x > 2.4$. Additionally, the amount of the pristine Alq₃ (O-*a*) decreases with deposition time. This supports the conclusion that the component O-*b* from the Al–O–C bond next to the phenoxide ring is the same in Alq₃, Alq₂ and Alq.

Fig. 5(a) shows the surface-sensitive N 1*s* core-level spectra taken at a photon energy of 440 eV during deposition of K onto a thick Alq₃ layer. The N 1*s* signal from pristine Alq₃ is located at ~ 400.2 eV, which shifts towards higher binding energy upon K deposition owing to band bending. A broad

Table 4

Binding energies and Gaussian widths of N 1*s* components and their corresponding area percentages.

Components	Evaporation time (min)	K concentration (x)	Binding energy (eV) N 1 <i>s</i>	Gaussian width (eV)	Area percentage (%)
N- <i>a</i>	0	0	400.18	1.18	100
	3	0.2	400.21	1.40	92.2
	9	0.7	400.35	1.42	75.2
	16	1.3	400.31	1.43	53.5
	21	1.7	400.30	1.43	43.3
	27	2.1	400.56	1.43	23.9
	31	2.4	400.68	1.45	17.6
	37	2.9	400.40	1.40	9.8
	45	3.5	400.53	1.42	9.0
	N- <i>b</i>	3	0.2	398.58	1.56
9		0.7	398.69	1.53	24.8
16		1.3	398.68	1.65	46.5
21		1.7	398.70	1.54	56.7
27		2.1	398.96	1.58	76.1
31		2.4	399.06	1.64	82.4
37		2.9	398.77	1.65	90.2
45		3.5	398.89	1.69	91.0

**Figure 5**

(a) Surface-sensitive N 1*s* core-level spectra taken *in situ* at a photon energy of 440 eV during deposition of K onto a thick Alq₃ layer. (b) Curve fit of the N 1*s* spectra in (a).

peak *C* clearly appears on the lower binding-energy side at $x = 0.7$. The broad peak *C* increases in intensity and becomes the dominant signal at higher K concentration. The observation of N 1*s* core-level spectra is consistent with previously published results (Greczynski *et al.*, 2000; Osada *et al.*, 1999). The bonding environments of N atoms can be further characterized *via* the fitted data in Fig. 5(b). Two N 1*s* components, N-*a* and N-*b*, are required to obtain a consistent fitted result for all the N 1*s* spectra. The binding-energy values and Gaussian widths of the two components are listed in Table 4. The component N-*a* is from pristine Alq₃, which is assigned from the N atom in the C=N–C bond in the pyridyl ring (Burrows *et al.*, 1996). The component N-*b* appears at $x = 0.2$, which increases in intensity with K concentration. Very probably the K-doped atoms generate a strained environment near the N atoms in the pyridyl ring in Alq₃ such that the C=N–C bond angle changes and results in the component N-*b*. At $x = 3.5$, N-*b* becomes the dominant signal. Note that no other N 1*s*-induced components appear at $x = 2.4$, 2.9 or 3.5, as was observed for the Al 2*p* components. This indicates that the cutting of C=N–C bonds in the pyridyl ring by the doped K atoms does not occur.

Note that the core-level spectra of K 2*p*, Al 2*p*, O 1*s* and N 1*s* shift towards higher binding energy upon K deposition, which is opposite to the photoemission screening effect. Similar to the work of Xu *et al.* (2002), the energy shift to higher binding energy is attributed to charge transfer in the initial state. The charge donated by K is considered to be delocalized in the valence band of Alq₃ since the K 2*p* core-level is also shifted to higher binding energy.

4. Conclusion

K is very reactive with Alq₃. A critical K concentration exists below which the K-doped atoms are near the O and N atoms within 8-quinolinoline ligands without bond cutting. Above the critical K concentration the Al–O–C bonds next to the

phenoxide ring are cut. An Alq_3 molecule may be disassembled into Kq and Alq_2 by bond cutting and bond formation. Alq_2 is likely to be further dissociated into Alq or even Al through subsequent formations of Kq .

The authors would like to thank Mr W. J. Lin and Mr Y. C. Wang for their technical assistance. The work was sponsored by the National Science Council through project NSC 96-2112-M-213-010-MY3.

References

- Brown, T. M., Friend, R. H., Millard, I. S., Lacey, D. J., Butler, T., Burroughes, J. H. & Cacialli, F. (2003). *J. Appl. Phys.* **93**, 6159–6172.
- Brundle, C. R. (1975). *Surf. Sci.* **48**, 99–136.
- Burrows, P. E., Shen, Z., Bulovic, V., McCarty, D. M., Forrest, S. R., Cronin, J. A. & Thompson, M. E. (1996). *J. Appl. Phys.* **79**, 7991–8006.
- Ganzorig, C., Suga, K. & Fujihira, M. (2001). *Mater. Sci. Eng. B*, **85**, 140–143.
- Greczynski, G., Fahlman, M., Salaneck, W. R., Johansson, N., dos Santos, D. A. & Brédas, J. L. (2000). *Thin Solid Films*, **363**, 322–326.
- Gredelj, S., Gerson, A. R., Kumar, S. & Cavallaro, G. P. (2001). *Appl. Surf. Sci.* **174**, 240–250.
- Haskal, E. I., Curioni, A., Seidler, P. F. & Andreoni, W. (1997). *Appl. Phys. Lett.* **71**, 1151–1153.
- Ishii, H., Sugiyama, K., Ito, E. & Seki, K. (1999). *Adv. Mater.* **11**, 605–625.
- Ishizaka, A. & Shiraki, Y. (1986). *J. Electrochem. Soc.* **133**, 666–671.
- Johansson, N., Osada, T., Stafström, S., Salaneck, W. R., Parente, V., dos Santos, D. A., Crispin, X. & Brédas, J. L. (1999). *J. Chem. Phys.* **111**, 2157–2163.
- Kido, J. & Matsumoto, T. (1998). *Appl. Phys. Lett.* **73**, 2866–2868.
- Kido, J., Nagai, K. & Okamoto, Y. (1993). *IEEE Trans. Electron Devices*, **40**, 1342–1344.
- Lee, J. H., Wu, M. H., Chao, C. C., Chen, H. L. & Leung, M. K. (2005). *Chem. Phys. Lett.* **416**, 234–237.
- López, M. F., Gutiérrez, A., García-Alonso, M. C. & Escudero, M. L. (1997). *Solid State Commun.* **101**, 575–580.
- Osada, T., Barta, P., Johansson, N., Kugler, Th., Bröms, P. & Salaneck, W. R. (1999). *Synth. Met.* **102**, 1103–1104.
- Parthasarathy, G., Shen, C., Kahn, A. & Forrest, S. R. (2001). *J. Appl. Phys.* **89**, 4986–4992.
- Schwieger, T., Peisert, H., Knupfer, M., Golden, M. S. & Fink, J. (2001). *Phys. Rev. B*, **63**, 165104.
- Stößel, M., Staudigel, J., Steuber, F., Blässing, J., Simmerer, J. & Winnacker, A. (2000). *Appl. Phys. Lett.* **76**, 115–117.
- Xu, B., Choi, J., Caruso, A. N. & Dowben, P. A. (2002). *Appl. Phys. Lett.* **80**, 4342–4344.
- Yeh, J. J. & Lindau, I. (1985). *Atom. Data Nucl. Data Tables*, **32**, 1–155.